Instrumented Indentation Testing

J.L. Hay, MTS Systems Corporation
G.M. Pharr, The University of Tennessee and Oak Ridge National Laboratory

INSTRUMENTED INDENTATION TESTING (IIT), also known as depth-sensing indentation, continuous-recording indentation, ultra-low-load indentation, and nanoindentation, is a relatively new form of mechanical testing that significantly expands on the capabilities of traditional hardness testing. Developed largely over the past two decades, IIT employs high-resolution instrumentation to continuously control and monitor the loads and displacements of an indenter as it is driven into and withdrawn from a material (Ref 1–13). Depending on the details of the specific testing system, loads as small as 1 nN can be applied, and displacements of 0.1 nm (1 Å) can be measured. Mechanical properties are derived from the indentation load-displacement data obtained in simple tests.

The advantages of IIT are numerous, as indentation load-displacement data contain a wealth of information, and techniques have been developed for characterizing a variety of mechanical properties. The technique most frequently employed measures the hardness, but it also gives the elastic modulus (Young's modulus) from the same data (Ref 8, 11). Although not as well-developed, methods have also been devised for evaluating the yield stress and strain-hardening characteristic of metals (Ref 14–16); parameters characteristic of damping and internal friction in polymers, such as the storage and loss modulus (Ref 17, 18); and the activation energy and stress exponent for creep (Ref 19–25). IIT has even been used to estimate the fracture toughness of brittle materials using optical measurement of the lengths of cracks that have formed at the corners of hardness impressions made with special sharp indenters (Ref 13, 26, 27). In fact, almost any material property that can be measured in a uniaxial tension or compression test can conceivably be measured, or at least estimated, using IIT.

An equally important advantage of IIT results because load-displacement data can be used to determine mechanical properties without having to image the hardness impressions. This facilitates property measurement at very small scales. Mechanical properties are routinely measured from submicron indentations, and with careful technique, properties have even been determined from indentations only a few nanometers deep. Because of this, IIT has become a primary tool for examining thin films, coatings, and materials with surfaces modified by techniques such as ion implantation and laser heat treatment.

Many IIT testing systems are equipped with automated specimen manipulation stages. In these systems, the spatial distribution of the near-surface mechanical properties can be mapped on a point-to-point basis along the surface in a fully automated way. Lateral spatial resolutions of about a micron have been achieved. An example of small indentations located at specific points in an electronic microcircuit is shown in Fig. 1.

The purpose of this article is to provide a practical reference guide for instrumented indentation testing. Emphasis is placed on the better-developed measurement techniques and the procedures and calibrations required to obtain accurate and meaningful measurements.

Testing Equipment

As shown schematically in Fig. 2, equipment for performing instrumented indentation tests consists of three basic components: (a) an indenter of specific geometry usually mounted to a rigid column through which the force is transmitted, (b) an actuator for applying the force, and (c) a sensor for measuring the indenter displacements. Because these are also the basic components used in tensile testing, a standard commercial tensile-testing machine can be adapted for IIT testing. However, to date, most IIT development has been performed using instruments specifically designed for small-scale work. Advances in instrumentation have been driven by technologies that demand accurate mechanical properties at the micron and submicron levels, such as the microelectronic and magnetic storage industries. Thus, while the principles and techniques described in this article were developed primarily using instruments designed for small-scale work, there is no inherent reason that they could not be ap-

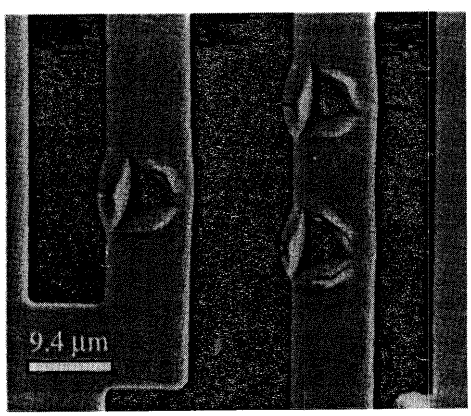

Fig. 1 Small Berkovich indentations located at specific positions in an electronic microcircuit

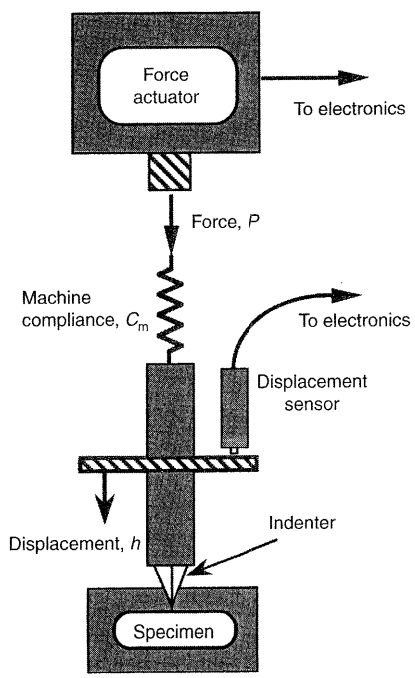

Fig. 2 Schematic representation of the basic components of an instrumented indentation testing system

plied at larger scales using equipment available in most mechanical-testing laboratories.

Several small-scale IIT testing systems are commercially available. They differ primarily in the ways the force is applied and the displacement is measured. Small forces can be conveniently generated (a) electromagnetically with a coil and magnet assembly, (b) electrostatically using a capacitor with fixed and moving plates, and (c) with piezoelectric actuators. The magnitudes of the forces are usually inferred from the voltages or currents applied to the actuator, although in piezoelectrically driven instruments, a separate load cell is often included to provide a direct measurement of the force. Displacements are measured by a variety of means, including capacitive sensors, linear variable differential transformers (LVDTs), and laser interferometers. The range and resolution of the instrument are determined by the specific devices employed.

It is important to realize that as in a commercial tensile-testing machine, the displacements measured in an IIT system include a component from the compliance of the machine itself. Under certain circumstances, the machine compliance can contribute significantly to the total measured displacement, so it must be carefully calibrated and removed from the load-displacement data in a manner analogous to tension and compression testing. Specific procedures for determining the machine compliance in IIT testing are outlined in this article.

A variety of indenters made from a variety of materials are used in IIT testing. Diamond is probably the most frequently used material because its high hardness and elastic modulus minimize the contribution to the measured displacement from the indenter itself. Indenters can be made of other less-stiff materials, such as sapphire, tungsten carbide, or hardened steel, but as in the case of the machine compliance, the elastic displacements of the indenter must be accounted for when analyzing the load-displacement data.

Pyramidal Indenters. The most frequently used indenter in IIT testing is the Berkovich indenter, a three-sided pyramid with the same depth-to-area relation as the four-sided Vickers pyramid used commonly in microhardness work. The Berkovich geometry is preferred to the Vickers because a three-sided pyramid can be ground to a point, thus maintaining its self-similar geometry to very small scales. A four-sided pyramid, on the other hand, terminates at a "chisel edge" rather than at a point, causing its small-scale geometry to differ from that at larger scales; even for the best Vickers indenters, the chisel-edge defect has a length of about a micron. Although Vickers indenters could conceivably be used at larger scales, their use in IIT has been limited because most work has focused on small-scale testing.

Spherical Indenters. Another important indenter geometry in IIT testing is the sphere. Spherical contact differs from the "sharp" contact of the Berkovich or Vickers indenters in the way in which the stresses develop during indentation. For spherical indenters, the contact stresses are initially small and produce only elastic deformation. As the spherical indenter is driven into the surface, a transition from elastic to plastic deformation occurs, which can theoretically be used to examine yielding and work hardening, and to recreate the entire uniaxial stress-strain curve from data obtained in a single test (Ref 14, 15). IIT with spheres has been most successfully employed with larger-diameter indenters. At the micron scale, the use of spherical indenters has been impeded by difficulties in obtaining high-quality spheres made from hard, rigid materials. This is one reason the Berkovich indenter has been the indenter of choice for most small-scale testing, even though it cannot be used to investigate the elastic-plastic transition.

Cube-Corner Indenters. Another indenter used occasionally in IIT testing is the cube-corner indenter, a three-sided pyramid with mutually perpendicular faces arranged in a geometry like the corner of a cube. The centerline-to-face angle for this indenter is 34.3°, whereas for the Berkovich indenter it is 65.3°. The sharper cube corner produces much higher stresses and strains in the vicinity of the contact, which is useful, for example, in producing very small, well-defined cracks around hardness impressions in brittle materials; such cracks can be used to estimate the fracture toughness at relatively small scales (Ref 13, 26, 27).

Conical Indenters. A final indenter geometry worth mentioning is the cone. Like the Berkovich, the cone has a sharp, self-similar geometry, but its simple cylindrical symmetry makes it attractive from a modeling standpoint. In fact, many modeling efforts used to support IIT are based on conical indentation contact (Ref 28–35). The cone is also attractive because the complications associated with the stress concentrations at the sharp edges of the indenter are absent. Curiously, however, very little IIT testing has been conducted with cones. The primary reason is that it is difficult to manufacture conical diamonds with sharp tips, making them of little use in the small-scale work around which most of IIT has developed (Ref 36). This problem does not apply at larger scales, where much could be learned by using conical indenters in IIT experimentation.

A summary of the indenters used in IIT testing and parameters describing their geometries is given in Table 1.

Table 1 Summary of nominal geometric relationships for several indenters used in IIT

Parameter	Vickers	Berkovich	Cube-corner	Cone (angle ψ)	Sphere (radius R)
Centerline-to-face angle, α	68°	65.3°	35.2644°	...	...
Area (projected), $A(d)$	24.504 d^2	24.56 d^2	2.5981 d^2	πa^2	πa^2
Volume-depth relation, $V(d)$	8.1681 d^3	8.1873 d^3	0.8657 d^3	...	...
Projected area/face area, A/A_f	0.927	0.908	0.5774	...	...
Equivalent cone angle, ψ	70.2996°	70.32°	42.28°	ψ	...
Contact radius, a	...	...	...	$d \tan \psi$	$(2Rd - d^2)^{1/2}$

Measurement of Hardness and Elastic Modulus

The two mechanical properties measured most frequently by IIT methods are hardness (H) and elastic modulus (Young's modulus) (E). A simple methodology has been developed by which these properties can be determined for isotropic materials exhibiting no time dependence in their deformation behavior, that is, no creep or viscoelasticity (Ref 11). For materials that do not experience pile-up, which includes most ceramics, hard metals, and soft metals that work harden, H and E can be determined generally within ±10%, sometimes better. The physical principles and models used to determine H and E from indentation load-displacement data are now discussed. Many of the basic principles also apply to the measurement of other properties discussed later in this article.

General Description of the Indentation Process. A schematic of the indentation process for an axisymmetric indenter of arbitrary profile is shown in Fig. 3. As the indenter is driven into the material, both elastic and plastic deformation processes occur, producing a hardness impression that conforms to the shape of the indenter to some contact depth, h_c. The radius of the circle of contact is a. As the indenter is withdrawn, only the elastic portion of the displacement is recovered, which effectively allows one to separate the elastic properties of the material from the plastic.

A schematic representation of indentation-load (P) versus displacement (h) data obtained during one full cycle of loading and unloading is presented in Fig. 4. The important quantities are the peak load (P_{max}), the maximum depth (h_{max}), the final or residual depth after unloading (h_f), and the slope of the upper portion of the unloading curve ($S = dP/dh$). The parameter

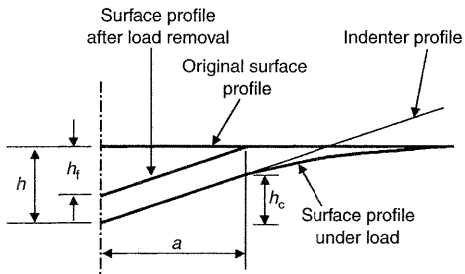

Fig. 3 Schematic representation of a section through an axisymmetric indentation showing various quantities used in analysis

S has the dimensions of force per unit distance and is known as the elastic contact stiffness, or more simply, the contact stiffness. The hardness and elastic modulus are derived from these quantities.

The fundamental relations from which H and E are determined are:

$$H = P/A \qquad \text{(Eq 1)}$$

where P is the load and A is the projected contact area at that load, and:

$$E_r = \frac{\sqrt{\pi}}{2\beta}\frac{S}{\sqrt{A}} \qquad \text{(Eq 2)}$$

where E_r is the reduced elastic modulus and β is a constant that depends on the geometry of the indenter (Ref 1, 11). Equation 1 is a working definition for the hardness as measured by instrumented indentation testing. By this definition, the hardness is a measure of the load-bearing capacity of the contact computed by dividing the applied load by the *projected area of contact under load.* This should not be confused with the more traditional definition of hardness: the load divided by *the projected area of contact of the residual hardness impression.* These two definitions yield similar values when plastic deformation processes dominate and a fully plastic permanent hardness impression is formed. However, they give very different values when contact is predominantly elastic, because for purely elastic contact, the residual contact area is vanishingly small, giving an infinite hardness based on the traditional definition. This subtle difference is especially important for indentations made with spherical indenters, for which purely elastic contact is commonly encountered, and for sharp indenters at very small depths where tip-rounding effects can produce predominantly elastic contact. Under these circumstances, the traditional definition of hardness yields a greater value than that obtained by Eq 1.

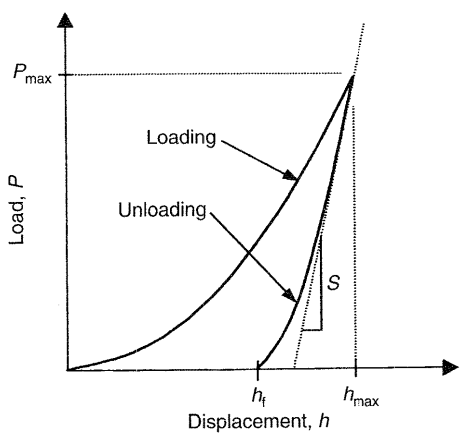

Fig. 4 Schematic representation of indentation load-displacement data during one complete cycle of loading and unloading

A reduced modulus, E_r, is used in Eq 2 to account for the fact that elastic displacements occur in both the indenter and the sample. The elastic modulus of the test material, E, is calculated from E_r using:

$$\frac{1}{E_r} = \frac{1-\nu^2}{E} + \frac{1-\nu_i^2}{E_i} \qquad \text{(Eq 3)}$$

where ν is the Poisson's ratio for the test material, and E_i and ν_i are the elastic modulus and Poisson's ratio, respectively, of the indenter. For diamond, the elastic constants E_i = 1141 GPa and ν_i = 0.07 are often used (Ref 11, 37). While it may seem counterintuitive that one must know the Poisson's ratio of the material in order to compute its modulus, even a rough estimate, say $\nu = 0.25 \pm 0.1$, produces only about a 5% uncertainty in the calculated value of E for most materials.

Equation 2 is founded in elastic contact theory (Ref 28, 29, 31) and holds for any indenter that can be described as a body of revolution of a smooth function (Ref 38). Because the equation was derived for an axisymmetric indenter, it formally applies only to circular contacts, for which the indenter geometry parameter is β = 1. However, it has been shown that the equation works equally well even when the geometry is not axisymmetric, provided that different values of β are used (Ref 39–41). For indenters with square cross sections like the Vickers pyramid, β = 1.012; for triangular cross sections like the Berkovich and the cube-corner indenters, β = 1.034 (Ref 39).

Very recent work has shown that yet another small correction factor to Eq 2 may be needed in very precise work (Ref 31, 42–45). Pending further development and verification, this correction is not considered in the procedures outlined here.

Determining the Contact Stiffness and Contact Area. From Eq 1 and 2, it is clear that in order to calculate the hardness and elastic modulus from indentation load-displacement data, one must have an accurate measurement of the elastic contact stiffness (S) and the projected contact area under load (A). One of the primary distinctions between IIT and conventional hardness testing is the manner in which the contact area is derived. Rather than by imaging, the area is established from an analysis of the indentation load-displacement data.

The most widely used method for establishing the contact area was developed by Oliver and Pharr (Ref 11), which expands on ideas suggested by several others (Ref 7, 8). The Oliver-Pharr method begins by fitting the unloading portion of the load-displacement data to the power-law relation:

$$P = BA(h - h_f)^m \qquad \text{(Eq 4)}$$

where B and m are empirically determined fitting parameters, and h_f is the final displacement after complete unloading, also determined from the curve fit. The contact stiffness (S) is established by analytically differentiating Eq 4 and evaluating the result at the maximum depth of penetration, $h = h_{max}$, that is:

$$S = \left(\frac{dP}{dh}\right)_{h=h_{max}} = Bm(h_{max} - h_f)^{m-1} \qquad \text{(Eq 5)}$$

Experience has shown that Eq 4 does not always provide an adequate description of the *entire* unloading curve, especially for films on substrates. In this case, using curve-fitting parameters based on all of the unloading data can lead to unacceptable errors in the contact stiffness computed from Eq 5. It is thus prudent practice to determine the contact stiffness by fitting only the upper portion of the unloading data; moreover, the value of S determined from this fit should be checked by comparing the curve fit to the data. Fitting the upper 25 to 50% of the data is usually sufficient.

The next step in the procedure is to determine the contact depth (h_c), which for elastic contact is less than the total depth of penetration (h_{max}) as illustrated in Fig. 3. The contact depth is estimated using:

$$h_c = h - \varepsilon\frac{P}{S} \qquad \text{(Eq 6)}$$

where ε is a constant that depends on the indenter geometry. Eq 6 is derived from an elastic contact analysis that shows that for spherical indenters $\varepsilon = 0.75$ and $h_c/h = 0.5$, and for conical indenters $\varepsilon = 0.72$ and $h_c/h = 2/\pi$ (Ref 11). Curiously, experiments with Berkovich indenters have shown that Eq 6 also works well for elastic-plastic indentation using ε = 0.75 (Ref 11). This observation has recently been explained using elastic-plastic contact analysis and finite element simulation (Ref 46). Note that Eq 6 does not account for the phenomenon of pile-up because its derivation is based strictly on elastic contact in which sink-in always occurs. The consequences of this assumption, which are important for materials in which pile-up is prevalent, are discussed later.

As a last step in the analysis, the projected contact area is calculated by evaluating an empirically determined indenter area function $A = f(d)$ at the contact depth h_c; that is:

$$A = f(h_c) \qquad \text{(Eq 7)}$$

The area function, $A = f(d)$, also known as the shape function or tip function, relates the cross-sectional area of the indenter (A) to the distance (d) from its tip. An experimental procedure for determining the area function is presented later in this article.

Once the projected contact area and contact stiffness are known, the hardness and elastic modulus follow from Eq 1 and 2.

Dynamic Stiffness Measurement. An important alternative for measuring the contact stiffness is offered by dynamic measurement techniques. Dynamic methods allow for the continuous measurement of stiffness as the indenter is driven in during loading (Ref 11, 47–49). The measurement is accomplished by

superimposing a small force oscillation on the primary loading signal and analyzing the resulting displacement response by means of a frequency-specific amplifier. The success of this technique relies on an accurate model for the dynamic response of the indentation system to allow for isolation of the material response. With dynamic stiffness measurement, one can obtain the hardness and elastic modulus as a continuous function of depth from a single indentation experiment. The technique is particularly useful for thin films, for which trends in H and E with depth provide important information about substrate influences on properties (Ref 50). For time-dependent materials, dynamic methods can also be used to explore rate sensitivity in the frequency domain (Ref 17, 18).

Influences of Pile-Up. The procedures outlined here for measuring hardness and elastic modulus are based entirely on elastic models of indentation contact. However, when sharp indenters like the Berkovich or Vickers are employed or when spherical indenters are used at larger loads, indentation is both elastic and plastic, and the plastic component sometimes has important consequences that cannot be explained by elastic models alone.

The most important plastic phenomenon is pile-up, where material plastically uplifts around the contact impression in a manner depicted schematically in Fig. 5. Pile-up does not occur in all materials. However, when it does, the contact area is larger than that predicted by elastic contact theory (material sinks in during purely elastic contact), and both H and E are overestimated because their evaluation depends on the contact area deduced from the load-displacement data (Eq 1, 2) (Ref 31, 51). Finite element simulation of indentation with conical indenters having the same depth-to-area relation as the Berkovich and Vickers has shown that the hardness can be overestimated by as much as 60% and the modulus by up to 30% (Ref 30, 31). The modulus is less severely affected because it is proportional to $1/\sqrt{A}$ (Eq 2), whereas the hardness depends on $1/A$ (Eq 1).

The types of materials and conditions for which pile-up is most likely to occur have been examined in finite element simulation (Ref 30, 31, 52). The fundamental material properties affecting pile-up are the ratio of the yield stress to modulus (σ_y/E) and the work-hardening behavior. In general, pile-up is greatest in materials with low σ_y/E and little or no capacity for work hardening, that is, "soft" metals that have been cold worked prior to indentation. The ability to work harden inhibits pile-up because as material adjacent to the indenter at the surface hardens during deformation, it constrains the upward flow of material to the surface.

Finite element simulations for conical indenters with half-included angles of 70.3° (the angle giving the same depth-to-area relation as the Berkovich and Vickers indenters) have shown that pile-up is not significant, irrespective of the work-hardening behavior, when $\sigma_y/E > 0.03$ (Ref 31). Unfortunately, because one usually does not know the value of σ_y/E for the material being tested, this parameter is of little practical value in assessing the potential for pile-up. However, finite element simulations have also shown that there is a strong correlation between σ_y/E and h_f/h_{max}, the ratio of the penetration depth upon unloading to the depth at maximum load. Because the latter parameter is directly measurable in an IIT test, it provides a useful means for determining when pile-up can be determined unimportant (Ref 31). Simulation results for a 70.3° conical indenter have shown that pile-up is minimal when $h_f/h_{max} < 0.7$; otherwise, pile-up may or may not be significant depending on the work-hardening behavior. Typical materials for which $h_f/h_{max} < 0.7$ are ceramics and the harder metals. A similar approach based on the ratio of the slopes of the loading and unloading curves (a quantity that can be measured continuously during loading using dynamic stiffness measurement) has also been developed (Ref 53).

As a practical matter, if there is suspicion that pile-up may be important based on the value of h_f/h_{max} and/or other independent knowledge of the properties of the material, indentations should be imaged to examine the extent of the pile-up and establish the true area of contact. Light microscopy, scanning electron microscopy (SEM), and atomic force microscopy (AFM) are all useful imaging techniques. For Berkovich or Vickers indenters, the edges of piled-up indentations have a distinct appearance; the sides of the residual hardness impression are bowed outwards as shown in Fig. 6. If pile-up is large, accurate measurements of H and E cannot be obtained using the contact area deduced from the load displacement data; rather, the area measured from the image should be used in Eq 1 and 2.

Thin Films. As mentioned in the introduction, one area in which IIT offers distinct advantages is in the measurement of thin-film mechanical properties. The measurement of films is more difficult than monolithic materials because the load-displacement data depend in complex ways on the properties of the film *and* the substrate on which it resides. Thus, obtaining absolute measurements of film properties is often difficult and requires careful data analysis.

The most common approach for isolating the film properties is to make measurements at depths that are such a small fraction of the film thickness that the behavior is essentially that of the material in bulk form. An often-used guideline is that the properties of the film may be evaluated independently of the substrate as long as the indentation depth is less than 10% of the film thickness (Ref 54). In actuality, the depth at which substrate-independent measurements are obtained depends in a complex way on the elastic and plastic properties of the film and substrate; thus, the guideline must be used with caution. The dynamic stiffness measurement technique is an especially useful tool for establishing the depth at which the measured properties are substrate independent. Because this method yields both the elastic modulus and the hardness as a continuous function of indenter penetration, the depths at which substrate influences are significant are often evident in dynamic stiffness data. For example, Fig. 7 shows the depth dependence of the hardness of a 1000 nm film of aluminum deposited

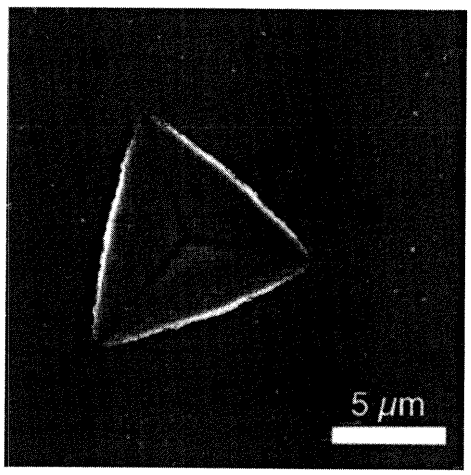

Fig. 6 Berkovich indentation in aluminum. The distinctly bowed-out edges of the contact indicate pile-up.

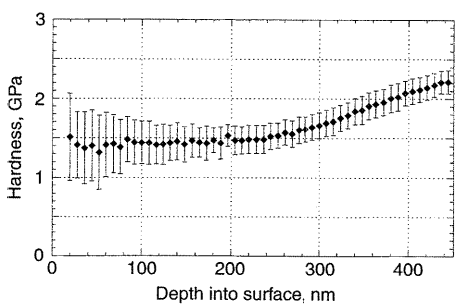

Fig. 7 Hardness versus indenter displacement for a 1000 nm aluminum film on silicon. The data indicate that the substrate influences the measured hardness at depths greater than 250 nm.

Fig. 5 Sink-in and pile-up during indentation

on silicon as measured by the dynamic stiffness technique. The constant hardness at depths below 250 nm indicates a true film hardness of about 1.4 GPa.

There are many measurement applications for which the film is so thin that substrate influences cannot be avoided at depths at which useful load-displacement data can be obtained. Under these circumstances, one must estimate the film properties from measurements of the composite structure. There are many empirical and analytic expressions for the composite hardness and elastic modulus that model the depth dependence of the composite film-substrate properties so as to allow extrapolation to the small depth limit (Ref 8, 33, 39, 55–63). However, most have not been tested using a broad range of materials. In one notable exception, a number of models were compared to an extensive set of experimental data for film-substrate systems (Ref 64). It was found that a model developed by Gao et al. works particularly well in predicting the depth dependence of the composite elastic modulus (E_c) of a film-substrate system with film thickness t_f (Ref 61). In this model, E_c is related to the modulus of the film (E_f) and the modulus of the substrate (E_s) through:

$$E_c = (E_f - E_s)\Phi + E_s \qquad \text{(Eq 8)}$$

where Φ is a weighting function that depends on the ratio of contact radius to film thickness ($x = a/t_f$) and Poisson's ratio (assumed to be the same for the film and substrate), through:

$$\Phi = \frac{2}{\pi}\arctan\frac{1}{x} + \frac{1}{2\pi(1-\nu)}\left[(1-2\nu)\frac{1}{x}\ln(1+x^2) - \frac{x}{1+x^2}\right] \qquad \text{(Eq 9)}$$

Given the linear form of Eq 8, a plot of E_c versus Φ has a slope of $(E_f - E_s)$ and an intercept of E_s, which can be used to deduce the modulus of the film if the modulus of the substrate is known. The conclusion that the model works well is based only on a comparison of the experimental data with the mathematical form of Eq 8 and 9; the model is yet to be fully evaluated using systems for which the modulus of the film and substrate are known independently of the indentation measurements.

Another promising technique for extracting film properties combines finite element simulations with experimental load-displacement data (Ref 35). To use this technique, one must independently know the elastic modulus, yield stress, and work-hardening behavior of the substrate. It is also necessary to know the thickness of the film and have a reasonable guess of the work-hardening behavior of the film. With this information, the film yield stress and modulus are guessed and adjusted in the finite-element code until the simulated load-displacement data match experiment. While subject to a number of potentially limiting assumptions, the technique is quite promising and merits further development.

Lastly, it should be noted that the pile-up and sink-in behavior of film-substrate systems can be very different from that of bulk materials in a manner that has important implications for IIT measurements. Recent experiments and finite-element simulations have shown that pile-up is significantly enhanced in soft films deposited on hard substrates due to constraint imposed on plastic deformation in the film by the substrate (Ref 58, 59, 65, 66). In addition, sink-in can be enhanced in hard films deposited on soft substrates due to yielding and plastic flow in the substrate (Ref 67). Examples of enhanced sink-in and pile-up are shown in Fig. 8. The limited available data suggest that the enhancements are greatest at penetration depths close to the film thickness. An important consequence is that the method for determining the contact area from Eq 5 to 7 breaks down in a manner that depends on the depth of penetration relative to the film thickness. For soft films on hard substrates, the enhancement of pile-up leads to an overestimation of H and E, just as it does for bulk soft metals with little or no work hardening. Such behavior is responsible for anomalously high elastic modulus measurements for soft aluminum films (H = 0.7 GPa) on hard glass substrates (H = 6.7 GPa) (Fig. 8a) (Ref 65). For hard films on soft substrates, sink-in is enhanced beyond what it would be for purely elastic contact, and the analysis overestimates the true contact area (Fig. 8b). This is the origin of smaller-than-expected elastic moduli measured for films of hard NiP (H = 7.5 GPa) deposited on soft annealed copper (H = 0.7 GPa) (Fig. 8b) (Ref 67).

For Berkovich indenters, clues to whether the enhancement of pile-up or sink-in occurs can be found in the shapes of hardness impressions. Enhancement of pile-up is evidenced by contact impression edges that bow outward due to a nonuniform distribution of the pile-up, which is greatest at the centers of the faces and smallest at the corners (Fig. 8a). Enhancement of sink-in produces the bowed-in appearance seen in Fig. 8(b). Collectively, these observations suggest that very complex elastic-plastic interactions occur in film-substrate systems, and that extreme care must be exercised in measuring their properties. To minimize these complications, measurements should be made, when possible, at small fractions of the film thickness, and the contact area and shape should be confirmed by imaging.

Time-Dependent Materials and Properties

All of the discussion so far has assumed that the material response to indentation contact is instantaneous, or nearly so, as is the case for most metals and ceramics tested at room temperature. In general, however, indentation deformation can be time-dependent, with the extent and nature of the time dependence strongly influenced by temperature. Time dependence is the rule rather than the exception in polymers—the viscoelastic behavior of polymers at room temperature is well known—and time-dependent creep is an important phenomenon in metals and ceramics at elevated temperatures. Methods for probing and characterizing the time-dependent phenomena, although not nearly as well developed as methods for measuring H and E, are now examined.

Influences on the Measurement of *H* and *E*. One important aspect of time-dependent behavior is an experimental complication arising in the measurements of hardness and modulus. Time-dependent creep and/or viscoelastic deformation can cause the indentation displacement to increase even as the indenter is unloaded, giving abnormally high contact stiffnesses that adversely affect the measurement of hardness and modulus. This is commonly encountered, for example, when testing soft metals, such as aluminum, with sharp

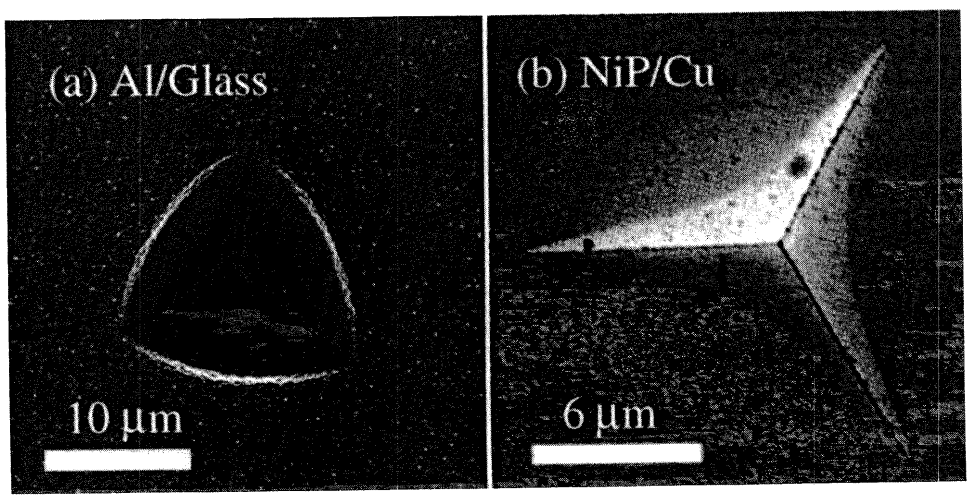

Fig. 8 Examples of sink-in and pile-up enhancement for thin films on substrates. (a) Soft aluminum on hard glass. Source: Ref 65. (b) Hard NiP on soft copper. Source: Ref 67

indenters like the Berkovich. In some cases, the time-dependent portion of the displacement can be large enough to produce an unloading curve with a negative slope. When creep is observed or suspected, holding the load constant for a period of time prior to unloading, which allows the creep displacements to dissipate, can help alleviate the problem, at least in materials with short-lived creep responses.

Measurement of Creep Parameters. For materials in which the creep response is dominant, IIT can be used to characterize and quantify important creep parameters. For conventional creep tests conducted in uniaxial tension, the temperature and stress dependence of the steady state creep rate ($\dot{\varepsilon}$) are often described by the relation:

$$\dot{\varepsilon} = \alpha\sigma^{n} \exp(-Q_c/RT) \qquad \text{(Eq 10)}$$

where α is a material constant, σ is stress, n is the stress exponent for creep, Q_c is the activation energy, R is the gas constant, and T is temperature. Values of n ranging from 3 to 5 are typical for many metals. By analogy, an equivalent expression can be developed for indentation creep conducted, for example, by applying a constant load to the indenter and monitoring its displacement as a function of time. The expression follows by defining an indentation strain rate as $\dot{\varepsilon}_i = \dot{h}/h$, that is, the normalized rate of indentation displacement (Ref 19, 24, 25). This definition is appropriate for cones and pyramids (Ref 9, 68). Noting that the equivalent of stress in an indentation test is the mean contact pressure $H = P/A$, the analog of Eq 10 for an indentation creep test is:

$$\dot{\varepsilon}_i = \alpha_i H^{n} \exp(-Q_c/RT) \qquad \text{(Eq 11)}$$

where α_i is a material constant.

Equation 11 has been found to adequately describe creep behavior of some but not all materials (Ref 19, 21–25, 68, 69). When it does, a log-log plot of the indentation strain rate versus hardness produces a straight line with a slope that gives the stress exponent, n. Interestingly, such a plot can often be constructed from data obtained in a single indentation test. As an example, consider the indentation creep data in Fig. 9 for indium, a material that creeps at room temperature by virtue of its relatively low melting point (Ref 25). The data were obtained by loading a Berkovich indenter at a fixed rate of loading and then holding at a maximum load while monitoring the indenter displacement as a function of time. As the indenter penetrates, the contact area increases (thereby reducing the contact pressure), and the rate of displacement decreases correspondingly. In a test like this, it is not unusual to obtain creep data over several orders of magnitude in $\dot{\varepsilon}_i$. The stress exponent deduced from the data, $n = 6$, is very close to the value derived using conventional creep testing techniques.

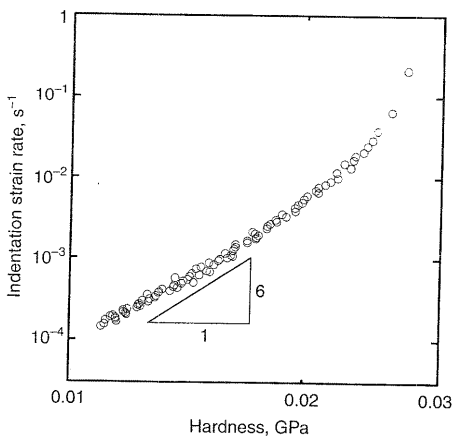

Fig. 9 Room-temperature indentation creep data for indium obtained by loading the indenter at a constant rate (10 mN/s) to a peak load and holding for an extended period of time. Source: Ref 25

To date, indentation creep tests have been limited largely to the low-melting metals that exhibit creep at room temperature. In some cases, the stress exponent measured by indentation techniques has been close to that determined in conventional tests, but in others it has not. One important reason for the difference concerns the influence of transients on the creep response. For an indentation creep test, the stresses in the vicinity of the contact vary with time and position as the indenter penetrates the specimen. Thus, transient effects (primary creep) and stress-induced changes in microstructure can influence the behavior in a manner that is not observed in uniaxial creep testing, for which the stress is relatively uniform and invariant with time. Carefully conducted indentation creep tests have shown that when $\dot{\varepsilon}_i$ varies significantly during the test, transient effects do indeed affect the results and are particularly important at high strain rates (Ref 25). It has been suggested that better results can be obtained by performing a series of tests over a range of $\dot{\varepsilon}_i$ in which the indentation strain rate in any one test is held constant. This is easily achieved in a displacement-controlled machine by maintaining $\dot{h}/h$ constant. Under conditions for which the deformation is predominantly steady state, a constant indentation strain rate can be obtained in a load-controlled system by holding the normalized loading rate $(\dot{P}/P)$ constant (Ref 25).

The effect of temperature on creep, as quantified by the activation energy (Q_c) has been investigated only to a very limited extent (Ref 23, 25, 68, 69). Such tests are challenging due to inherent difficulties in measuring small displacements at elevated temperatures. When the specimen and/or testing apparatus are heated, the measured displacements are often dominated by thermal expansions and contractions of the machine, which are difficult to separate from the data.

Viscoelasticity. In addition to creep, indentation techniques have also been developed to characterize the time-dependent properties of viscoelastic materials like polymers. Dynamic stiffness measurement techniques offer distinct advantages here. Using the amplitude and phase of the force and displacement oscillations, the storage modulus (E'), characteristic of elasticity, and the loss modulus (E''), characteristic of internal friction and damping, can both be measured (Ref 17, 18). In its simplest form, the analysis follows by modeling the contact as a spring of stiffness S in parallel with a dashpot with damping coefficient $C\omega$, where ω is the angular frequency of the dynamic oscillation. Provided the dynamic response of the testing system is well known, S and $C\omega$ can be measured from the amplitude and phase of the load and displacement oscillations. The storage modulus is related to S by Eq 2; that is:

$$E' = \frac{\sqrt{\pi}}{2\beta}\frac{S}{\sqrt{A}} \qquad \text{(Eq 12)}$$

and by analogy to this equation, it has been suggested that the loss modulus is related to $C\omega$ through:

$$E'' = \frac{\sqrt{\pi}}{2\beta}\frac{C\omega}{\sqrt{A}} \qquad \text{(Eq 13)}$$

Other models for the dynamic response of the specimen-indenter contact can be used to give similar results.

Although quite promising, the technique has yet to be rigorously tested on a variety of materials. Thus far, only materials with exceptionally high damping, like natural rubber, have been examined.

Good Experimental Practice

As in any experimental work, accurate measurements can be obtained only with good experimental technique and practice. A discussion of some of the factors that should be considered in making high-quality measurements follows. Emphasis is placed on those that are common to many measurement procedures and independent of the specific apparatus used to make them.

Choosing an appropriate indenter requires consideration of a number of factors. One consideration is the strain the tip imposes on the test material. Although the indentation process produces a complex strain field beneath the indenter, it has proven useful to quantify the field with a single quantity, often termed the characteristic strain (ε) (Ref 70, 71). Empirical studies in metals have shown that the characteristic strain can be used to correlate the hardness to the flow stress in a uniaxial compression test (Ref 70). For sharp indenters, such as self-similar cones and pyramids, the characteristic strain is constant regardless of the load or displacement, and is given by:

$$\varepsilon = 0.2 \cot(\psi) \qquad \text{(Eq 14)}$$

where ψ is the half-included angle of the indenter for cones; for pyramids, ψ is the half-included angle of the cone having the same area-to-depth relationship (Ref 70, 71). Thus, the sharper the cone or pyramid, the larger the characteristic strain. For the two most commonly used pyramidal indenters, the Berkovich and Vickers, the characteristic strain is about 8%, and the measured hardness is about 2.8 times the stress measured at 8% strain in a uniaxial compression test.

The use of sharper pyramidal indenters (smaller centerline-to-face angles), such as the cube-corner, is required when one wishes to produce larger strains. For example, cube-corner indenters are preferred to Berkovich indenters when investigating fracture toughness at small scales by indentation-cracking methods because the larger strain induces cracking at much smaller loads (Ref 13, 26, 27). There are problems, however, in obtaining accurate measurements of hardness and elastic modulus with cube-corner indenters (Ref 43–45). Although not entirely understood, the problems appear to have two separate origins. First, as the angle of the indenter decreases, friction in the specimen-indenter interface and its influence on the contact mechanics becomes increasingly important. Second, as mentioned earlier, recent analytical work has shown that Eq 2 is not an entirely adequate description of the relation among the contact stiffness, contact area, and reduced elastic modulus (Ref 42–45). Corrections are required, and the magnitude of the correction factor depends on angle of the indenter. The correction is relatively small for the Berkovich indenter, but much greater for the cube-corner indenter. Future measurement of H and E with cube-corner indenters will require methods for dealing with these complications (Ref 45).

For spherical indenters, the characteristic strain changes continuously as the indenter penetrates the material, as given by:

$$\varepsilon = 0.2a/R \qquad \text{(Eq 15)}$$

where a is the radius of contact and R is the radius of the indenter (Ref 71). Thus, spheres can be used when one wishes to take advantage of the continuously changing strain. In principle, one can determine the elastic modulus, yield stress, and strain-hardening behavior of a material all in one test. However, because plasticity commences well below the surface (Ref 70–73), the point of initial yielding can be difficult to detect experimentally. Specific methods for exploring the stress-strain curve with spherical indenters are described elsewhere (Ref 14–16, 70).

It is important to note that in order to measure a value for the hardness that is consistent with the traditional definition—that is, the indentation load normalized by the area of the *residual* hardness impression—the contact must be fully plastic. For spherical indenters, full plasticity is achieved in elastic-perfectly-plastic materials when $E_r a/\sigma_y R > 30$ (Ref 71). Thus, the contact radius (a) and, therefore, the penetration depth at which full plasticity is achieved are smaller for spherical indenters with smaller radii (R). This is one important reason that sharp pyramids, such as the Berkovich, are often preferred to spheres for small depth testing. The tip radii on precision-ground Berkovich indenters are usually no greater than 100 nm—often better—implying that fully plastic contact is achieved at very small depths. Table 1 provides useful information on indenter geometries commonly used in IIT testing.

Environmental Control. To take full advantage of the fine displacement resolution available in most IIT testing systems, several precautions must be taken in choosing and preparing the testing environment. Uncertainties and errors in measured displacements arise from two separate environmental sources: vibration and variations in temperature that cause thermal expansion and contraction of the sample and testing system.

To minimize vibration, testing systems should be located on quiet, solid foundations (ground floors) and mounted on vibration-isolation systems. Thermal stability can be provided by enclosing the testing apparatus in an insulated cabinet to thermally buffer it from its surroundings and by controlling room temperature to within ±0.5 °C. If the material is thermally stable (i.e., not time dependent), one can account for small thermal displacements using procedures described later. However, for time-dependent materials, extra care must be taken in providing thermal stability, because separation of the thermal displacements from the specimen displacements is virtually impossible and, therefore, introduces large uncertainties into the displacement data.

Surface Preparation. Surface roughness is extremely important in instrumented indentation testing because the contact areas from which mechanical properties are deduced (for instance, using Eq 5–7) are calculated from the contact depth and area function *on the presumption that the surface is flat.* Thus, the allowable surface roughness depends on the anticipated magnitude of the measured displacements and the tolerance for uncertainty in the contact area. The greatest problems are encountered when the characteristic wavelength of the roughness is comparable to the contact diameter. In this case, the contact area determined from the load-displacement data underestimates the true contact area for indentations residing in "valleys" and overestimates it for indentations on "peaks." The magnitude of the error depends on the wavelength and amplitude of the roughness relative to the contact dimensions. Thus, one should strive to prepare the specimen so that the amplitude of the roughness at wavelengths near the contact dimension is minimized. For metallographic specimens, a good guide for surface preparation is ASTM E 380 (Ref 74). One can normally determine whether roughness is an issue by performing multiple tests in an area and examining the scatter in measured properties. For a homogeneous material with minimal roughness, scatter of less than a few percent can be expected with a good testing system and technique.

Testing Procedure. To avoid interference, successive indentations should be separated by at least 20 to 30 times the maximum depth when using a Berkovich or Vickers indenter. For other geometries, the rule is 7 to 10 times the maximum contact radius. The importance of frequently testing a standard material cannot be overemphasized. For reasons explained in the calibration section, fused quartz is a good choice for such a standard. It is good practice to routinely perform 5 to 10 indents on the standard; when the measured properties of the standard appear to change, the user is immediately alerted to problems in the testing equipment and/or procedures.

Detecting the Surface. One very important part of any good IIT testing procedure is accurate identification of the location of the surface of the specimen. This is especially important for very small contacts, for which small errors in surface location can produce relatively large errors in penetration depth that percolate through the calculation procedures to all those properties derived from the load-displacement data (Ref 75). Schemes for detecting the surface are frequently based on the change in a contact-sensitive parameter that is measured continuously as the indenter approaches the surface. For hard and stiff materials, such as hardened metals and ceramics, the load and/or contact stiffness, both of which increase upon contact, are often used. However, for soft, compliant materials, like polymers and biological tissues, the rate of increase in load and contact stiffness is often too small to allow for accurate surface identification. In these situations, a better method is sometimes offered by dynamic stiffness measurement, for which the phase shift between the load and displacement oscillations can potentially provide a more sensitive indication of contact, depending on the dynamics of the testing apparatus and the properties of the material (Ref 48, 49).

Calibrations

The accurate measurement of mechanical properties by IIT requires well-calibrated testing equipment. While load and displacement calibrations are usually provided by the manufacturer using procedures specific to the machine, a number of calibrations must be routinely performed by the user. These calibrations are discussed in an order that roughly reflects the frequency of their necessity; that is, thermal-drift calibration is performed most often. With minor modifications, the procedures are essentially those developed by Oliver and Pharr (Ref 11).

Many of the calibrations require that a calibration material be indented during the procedure. One material commonly used for this pur-

pose is fused quartz. This relatively inexpensive material is readily available in a highly polished form that gives repeatable results with very little scatter. Due to its amorphous nature, it is highly isotropic, and its relatively low elastic modulus, (E = 72 GPa) and high hardness (H = 9 GPa), facilitate calibrations that are best served by a large elastic recovery during unloading, such as area-function calibrations. Pile-up is not observed in fused quartz, and because it is not subject to oxidation, its near-surface properties are similar to those of the bulk and do not depend to a large degree on the depth of penetration. Fused quartz also exhibits essentially no time dependence when indented at room temperature, so there are no complications in separating thermal drift from time-dependent deformation effects.

Thermal-Drift Calibration. Thermal drift calibration seeks to adjust the measured displacements to account for small amounts of thermal expansion or contraction in the test material and/or indentation equipment. Good technique requires that it be performed individually for each indentation because the drift rate can vary in relatively short time spans. In fact, the calibration is best achieved by incorporation directly into the indentation test procedure itself. A procedure that works well for materials exhibiting little or no time-dependent deformation behavior (metals and ceramics tested at room temperature) is based on the notion that displacements observed when the indenter is pressed against the sample surface at a small, fixed load must arise from thermal drift. This can be implemented in an indentation experiment by including a period near the end of the test during which the load is held constant for a fixed period of time (about 100 seconds is usually sufficient) while the displacements are monitored to measure the thermal-drift rate. A small load is preferred to minimize the possibility of creep in the specimen; a good guideline for this load is 10% of the maximum indentation load. Displacement changes measured during this period are attributed to thermal expansion or contraction in the test material and/or indentation equipment, and a drift rate is calculated from the data. All displacements measured during the indentation test are then corrected according to the time at which they were acquired. For example, if the measured thermal drift rate is +0.05 nm/s, then a displacement acquired 10 s into the experiment must be corrected by –0.5 nm.

Figure 10 shows displacement-versus-time data acquired during a constant load period near the end of a test in fused quartz. In this case, the drift rate was fairly high, about 0.31 nm/s. Figure 11 shows the effect of applying this correction to the indentation load-displacement data. The shift in the corrected load-displacement curves has important consequences for the calculated contact area by affecting the maximum depth of penetration and the contact depth. Although not quite as obvious, the thermal drift also affects the contact stiffness determined from the slope of the unloading curve.

If the test material exhibits significant time-dependent deformation, as might be the case for polymers or metals tested at a significant fraction of their melting point, thermal drift correction should not be used because it is not possible to distinguish the thermal displacements from time-dependent deformation in the specimen. Under such circumstances, thermal drift should be minimized by precisely controlling the temperature of the testing environment and allowing samples to thermally equilibrate for long periods of time prior to testing.

Machine Compliance (Stiffness) Calibration. Determination of the machine compliance (C_m) or equivalently, the machine stiffness ($K_m = 1/C_m$) allows one to determine that part of the total measured displacement (h_t) that occurs in the test equipment and correct the indentation data for it. If C_m or K_m is known, then the displacement in the machine at any load (P) is simply $h_m = C_m P = P/K_m$, and the true displacement in the specimen is given by:

$$h = h_t - C_m P = h_t - P/K_m \qquad \text{(Eq 16)}$$

To determine C_m or K_m, the machine and contact are modeled as springs in series whose compliances are additive. Thus, the total measured compliance (C_t) is given by:

$$C_t = C_s + C_m \qquad \text{(Eq 17)}$$

where C_s is the elastic compliance of the indenter-specimen contact. Because C_t is just the inverse of the total measured stiffness (S_t), and

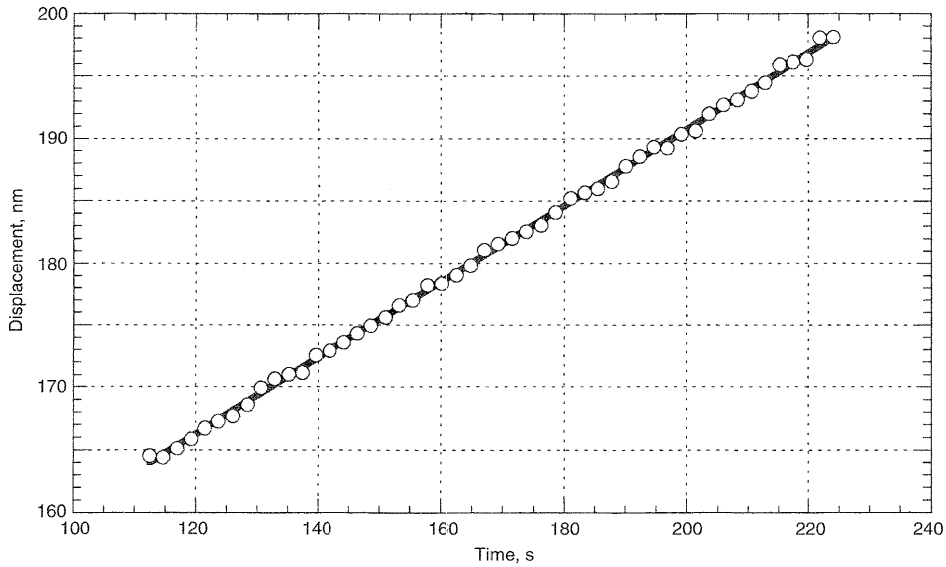

Fig. 10 Indenter displacement versus time during a period of constant load showing thermal drift in a fused quartz specimen. The measured drift rate, 0.31 nm/s, is used to correct the load-displacement data shown in Fig. 11.

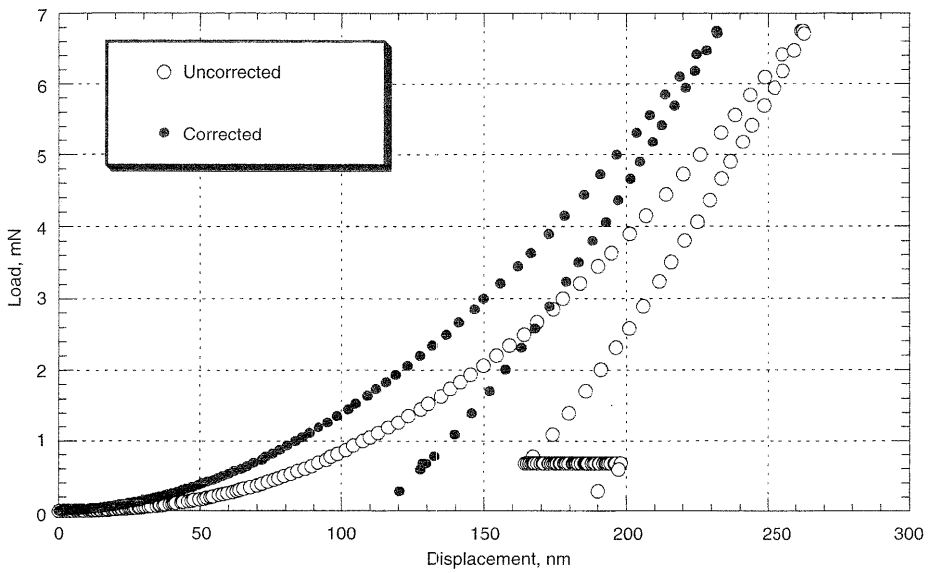

Fig. 11 Load-displacement data for fused quartz showing correction for thermal drift

C_s is the inverse of the elastic contact stiffness (S), Eq 2 and 17 combine to yield:

$$C_t = \frac{\sqrt{\pi}}{2\beta E_r}\frac{1}{\sqrt{A}} + C_m \qquad \text{(Eq 18)}$$

Thus, the intercept of a plot of C_t versus $A^{-1/2}$ gives the machine compliance (C_m) and the slope of the plot is related to the reduced modulus (E_r). Because extrapolation of the data to $A^{-1/2} = 0$ is required, the best measures of C_m are obtained when the first term on the right is small, that is, for large contacts.

A convenient procedure for determining C_m is based on the assumption that the area function of the indenter at large depths is well described by the ideal area function, that is, the area function under the assumption that the indenter has no deviations from its perfect geometric shape. For pyramidal and conical indenters, the ideal area function is given by:

$$A = F_1 d^2 \qquad \text{(Eq 19)}$$

where the constant F_1 follows from geometry. Values of F_1 for several important indenters are included in Table 1. For spherical indenters, the ideal area function depends on the diameter of the sphere (D) through:

$$A = \pi d(D - d) = -\pi d^2 + \pi D d \qquad \text{(Eq 20)}$$

which, for small penetration depths relative to the sphere diameter ($d < D$), simplifies to:

$$A = \pi D d = F_2 d \qquad \text{(Eq 21)}$$

where $F_2 = \pi D$.

The specific calibration procedure used to determine the machine compliance is an iterative one that uses data from a calibration material such as fused quartz. Indentations are made at several large depths for which the ideal area function is expected to apply. Assuming first that $C_m = 0$, the load-displacement data are corrected for the machine compliance according to Eq 16 and analyzed according to Eq 4–7 to determine the contact area at each depth. The intercept of a plot of C_t versus $A^{-1/2}$ then gives a new estimate of C_m. After correcting the load-displacement data for the new C_m, which affects the values of $A^{-1/2}$, the procedure is iteratively repeated until adequate convergence in C_m is obtained. As a check on the procedure, the slope of the final C_t versus $A^{-1/2}$ plot should be within a few percent of $\sqrt{\pi}/(2\beta E_r)$, as indicated in Eq 18. If not, one must question whether the assumed ideal geometry is correct and carefully inspect the indenter to check on it.

Accurately knowing C_m and K_m becomes increasingly important as the contact stiffness (S) approaches the machine stiffness (K_m). Because S increases with $\sqrt{A}$, machine stiffness corrections are most important for larger contacts. For example, Fig. 12 shows the effect of K_m on load-displacement data for relatively small and large indentations in fused quartz obtained with a Berkovich indenter. In each plot, the data have been reduced in two ways: (a) using $K_m = 1 \times 10^{30}$ N/m, that is, an essentially infinite machine stiffness; (b) using the correct value, $K_m = 6.8 \times 10^6$ N/m. The data in Fig. 12(a) are largely unaffected by the machine stiffness correction because the small load ($P_{max} = 7$ mN) is associated with a small contact stiffness; in this case, the contact stiffness is less than 1% of K_m. In Fig. 12(b), however, the machine stiffness correction is much more important because the contact stiffness at the larger peak load, 600 mN, is approximately 10% of the machine stiffness. One sure symptom of an incorrect K_m is a steady change in E with depth in a sample that should have depth-independent properties. Assuming all else is correct, if one uses a value of K_m that is too large, E will be correct at small depths, but will steadily decrease at larger depths; the converse is also true.

Area-Function Calibration. Although the ideal area function sometimes provides an accurate description of the contact geometry, especially at larger contact depths, deviations from geometrical perfection near the indenter tip, even when subtle, must be properly taken into account when measurements are to be made at small scales. For pyramidal indenters and cones, variations from the ideal self-similar geometry are produced by tip blunting. For spherical indenters, knowledge of the precise tip shape is important because small deviations from perfect spherical geometry can have large effects on the measured contact area. There may also be circumstances for which the ideal area function is not known, as in the case of a pyramidal indenter not ground precisely to the appropriate face angles. In each of these situations, the area function must be determined by an independent method. A general procedure for calibrating area functions without having to image the indenter or contact impressions follows.

The area function is determined by making a series of indentations at various depths in a calibration material of well-known elastic properties. The data can also be acquired using dynamic stiffness measurement, which has the advantage of being able to obtain all the necessary data in a few tests. The basic assumption is that the elastic modulus is independent of depth, so it is imperative that a calibration material be chosen that is free of oxides and other surface contaminants that may alter the near-surface elastic properties. It is also imperative that there be no pile-up, because the procedure is based on Eq 4–7, which do not account for the influences of pile-up on the contact depth. For these reasons, fused quartz is a good choice, although because of its relatively high hardness (H = 9 GPa), the upper limit on the achievable depth is somewhat restricted. For the specific procedure outlined here, the machine compliance must also be known from the procedures outlined in the previous section. In cases for which this is not possible, as when the ideal area function is not known or suspected to be inaccurate, an alter-

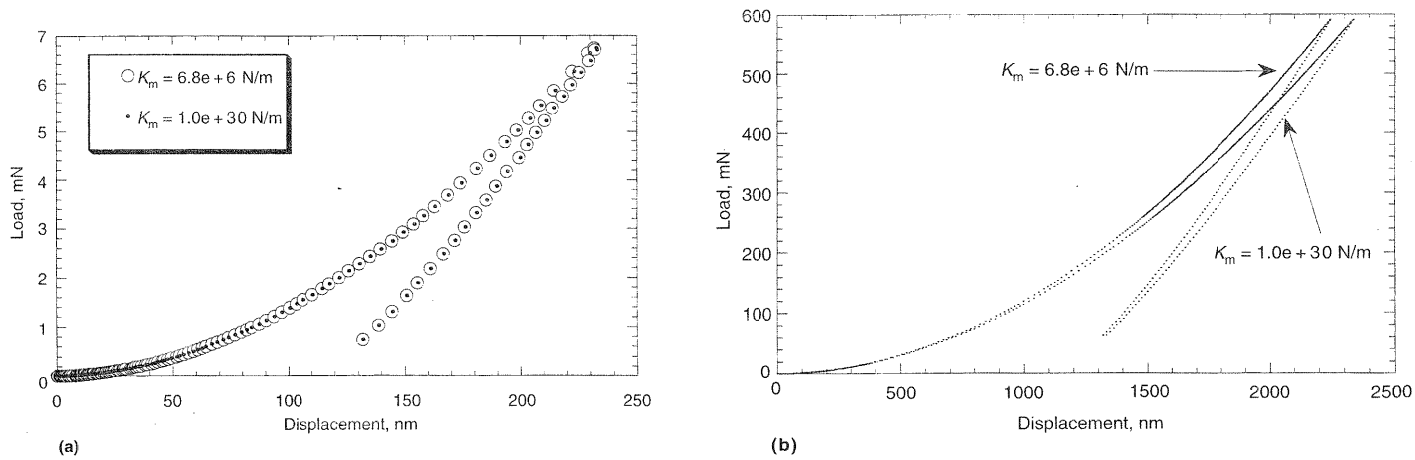

Fig. 12 Load-displacement data for fused quartz showing machine stiffness corrections at two peak loads: (a) 7 mN and (b) 600 mN. The correct machine stiffness is 6.8×10^6 N/m, while the value $K_m = 1 \times 10^{30}$ is used to represent an infinite stiffness. The plots illustrate the insensitivity of the load-displacement data to machine stiffness corrections for small contacts, but the stiffness correction is more important when the contact is large.

native procedure must be adopted in which the machine compliance and the area function are determined simultaneously in a coupled, iterative process. This procedure, which is considerably more complex, is described in detail elsewhere (Ref 11).

To implement the area-function calibration, a series of indentations is made at depths spanning the range of interest, usually from as small as possible to as large as possible, so that the area function is established over a wide range. Correcting for machine compliance, the load-displacement data are reduced and used to obtain the contact stiffnesses (S) and the contact depths (h_c) by means of Eq 5 and 6. From these quantities and the known elastic properties of the calibration material, the contact areas are determined by rewriting Eq 2 as:

$$A = \frac{\pi}{4}\left(\frac{S}{\beta E_r}\right)^2 \qquad \text{(Eq 22)}$$

When fused quartz is used as the calibration material (E = 72 GPa; ν = 0.17) and the indenter is diamond (E = 1141 GPa; ν = 0.07), the reduced modulus in the above expression is E_r = 69.6 GPa. A plot of A versus h_c then gives a graphical representation of the area function, which can be curve fit according to any of a number of functional forms. A general form that is often used is:

$$A = C_1 d^2 + C_2 d + C_3 d^{1/2} + C_4 d^{1/4} + C_5 d^{1/8} + \ldots \qquad \text{(Eq 23)}$$

where the number of terms is chosen to provide a good fit over the entire range of depths as assessed by comparing a log-log plot of the fit with the data. Because data are often obtained over more than one order of magnitude in depth, a weighted fitting procedure should be used to assure that data from all depths have equal importance. Note that the first term in the expression represents the ideal area function for a pyramidal or conical indenter provided $C_1 = F_1$ in Eq 19. Thus, for pyramidal and conical indenters for which the ideal area function is known, it is often convenient to fix $C_1 = F_1$.

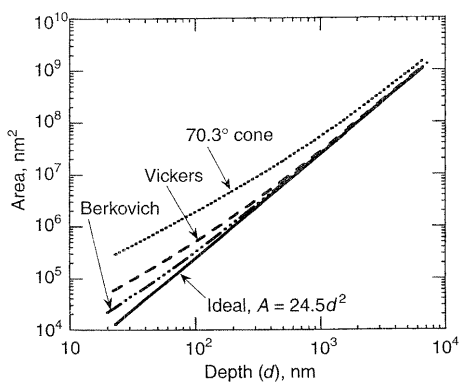

Fig. 13 Calibrated area functions for three indenters. Although the ideal area function, $A = 24.5d^2$, is nominally the same for each, the area functions differ due to different degrees of tip rounding. Source: Ref 36

Similarly, inspection of Eq 20 shows that for spherical indenters of known diameter D, one may wish to set $C_1 = -\pi$ and $C_2 = \pi D$. Fixing the values of these constants is particularly important when areas greater than those achievable in the calibration material are to be determined by extrapolating the area function to larger depths. Such extrapolations should be used with caution and only when there is confidence that the ideal area function applies at large depths. At depths greater than those included in the calibration, it is usually best to use the ideal area function of the indenter.

Figure 13 shows area functions determined with these procedures for three separate diamond indenters: Berkovich, Vickers, and a 70.3° cone (Ref 36). All three have nominally the same ideal area function, $A = 24.5\ d^2$, and tend to this function at large depths. However, the data show that there is indeed tip blunting for all three indenters, the conical diamond having the most and the Berkovich the least. The data corroborate the claim that the sharpest diamonds are those with the Berkovich geometry.

Future Trends

Instrumented indentation testing is a dynamic, growing field for which many new developments can be expected in the near future. From an equipment standpoint, one can expect that conventional microhardness testing equipment will be adapted to expand its capabilities in the manners afforded by IIT. This will lead to a new generation of relatively inexpensive IIT testing systems that operate primarily in the microhardness regime. Integration of atomic force microcopy with IIT will become increasingly more commonplace, allowing one to obtain three-dimensional images of small indentations to confirm contact areas and to examine pile-up phenomena. New displacement measurement methods based on laser interferometry can be expected to improve displacement measurement resolution and reduce the influences of machine compliance and thermal drift on measured properties. Laser interferometry will also facilitate testing at nonambient temperatures.

One can also expect new developments in techniques for measurement and analysis. Finite-element simulation may become an integral part of property measurement, accounting for the influences of pile-up and aiding the separation of film properties from substrate influences. Finite-element techniques may also prove useful in establishing tensile stress-strain behavior from experimental data obtained with spherical indenters. New methods and analyses based on dynamic measurement techniques can be expected to expand the characterization of the viscoelastic behavior of polymers over a wide range of frequency.

One of the great challenges in IIT is to develop equipment and techniques for measuring the properties of ultra-thin films, such as the hard protective overcoats used in magnetic disk storage, some of which are only 5 nm thick. At these scales, surface contaminants and surface forces due to absorbed liquid films severely complicate contact phenomena and analyses. New methods for obtaining and analyzing such data will be required.

ACKNOWLEDGMENTS

This work was sponsored in part by the Division of Materials Sciences, U.S. Department of Energy, under contract DE-AC05-96OR22464 with Lockheed Martin Energy Research Corp. and through the SHaRE Program under contract DE-AC05-76OR00033 with Oak Ridge Associated Universities.

REFERENCES

1. S.I. Bulychev, V.P. Alekhin, M.Kh. Shorshorov, A.P. Ternovskii, and G.D. Shnyrev, Determining Young's Modulus from the Indenter Penetration Diagram, *Zavod. Lab.*, Vol 41 (No. 9), 1975, p 1137–1140
2. F. Frohlich, P. Grau, and W. Grellmann, Performance and Analysis of Recording Microhardness Tests, *Phys. Status Solidi (a)*, Vol 42, 1977, p 79–89
3. M. Kh. Shorshorov, S.I. Bulychev, and V.P. Alekhin, Work of Plastic Deformation during Indenter Indentation, *Sov. Phys. Dokl.*, Vol 26 (No. 8), 1982, p 769–771
4. D. Newey, M.A. Wilkens, and H.M. Pollock, An Ultra-Low-Load Penetration Hardness Tester, *J. Phys. E, Sci. Instrum.*, Vol 15, p 119–122
5. J.B. Pethica, R. Hutchings, and W.C. Oliver, Hardness Measurements at Penetration Depths as Small as 20 nm, *Philos. Mag. A*, Vol 48 (No. 4), 1983, p 593–606
6. W.C. Oliver, Progress in the Development of a Mechanical Properties Microprobe, *MRS Bull.*, Vol 11 (No. 5), 1986, p 15–19
7. J.L. Loubet, J.M. Georges, O. Marchesini, and G. Meille, Vickers Indentation Curves of MgO, *J. Tribology (Trans. ASME)*, Vol 106, 1984, p 43–48
8. M.F. Doerner and W.D. Nix, A Method for Interpreting the Data from Depth-Sensing Indentation Instruments, *J. Mater. Res.*, Vol 1, 1986, p 601–609
9. H.M. Pollock, D. Maugis, and M. Barquins, "Characterization of Sub-Micrometer Layers by Indentation," ASTM STP 889, *Microindentation Techniques in Materials Science and Engineering*, P.J. Blau and B.R. Lawn, Ed., ASTM, 1986, p 47–71
10. W.D. Nix, Mechanical Properties of Thin Films, *Metall. Trans. A*, Vol 20, 1989, p 2217–2245
11. W.C. Oliver and G.M. Pharr, An Improved Technique for Determining Hardness and Elastic Modulus Using Load and Displace-

ment Sensing Indentation Experiments, *J. Mater. Res.*, Vol 7 (No. 6), 1992, p 1564–1583
12. G.M. Pharr and W.C. Oliver, Measurement of Thin Film Mechanical Properties Using Nanoindentation, *MRS Bull.*, Vol 17, 1992, p 28–33
13. G.M. Pharr, Measurement of Mechanical Properties by Ultra-low Load Indentation, *Mater. Sci. Eng. A*, Vol 253, 1998, p 151–159
14. J.S. Field and M.V. Swain, A Simple Predictive Model for Spherical Indentation, *J. Mater. Res.*, Vol 8 (No. 2), 1993, p 297–306
15. J.S. Field and M.V. Swain, Determining the Mechanical Properties of Small Volumes of Material from Submicron Spherical Indentations, *J. Mater. Res.*, Vol 10 (No. 1), 1995, p 101–112
16. M.V. Swain, Mechanical Property Characterization of Small Volumes of Brittle Materials with Spherical Tipped Indenters, *Mater. Sci. Eng. A*, Vol 253, 1998, p 160–166
17. J.-L. Loubet, B.N. Lucas, and W.C. Oliver, Some Measurements of Viscoelastic Properties with the Help of Nanoindentation, *NIST Special Publication 896: International Workshop on Instrumented Indentation*, 1995, p 31–34
18. B.N. Lucas, C.T. Rosenmayer, and W.C. Oliver, Mechanical Characterization of Sub-Micron Polytetrafluoroethylene (PTFE) Thin Films, in *Thin Films—Stresses and Mechanical Properties VII, MRS Symposium Proc.*, Vol 505, Materials Research Society, 1998, p 97–102
19. M.J. Mayo and W.D. Nix, A Microindentation Study of Superplasticity in Pb, Sn, and Sn-38wt%Pb, *Acta Metall.*, Vol 36 (No. 8), 1988, p 2183–2192
20. M.J. Mayo, R.W. Siegel, A. Narayanasamy, and W.D. Nix, Mechanical Properties of Nanophase TiO_2 as Determined by Nanoindentation, *J. Mater. Res.*, Vol 5 (No. 5), 1990, p 1073–1082
21. V. Raman and R. Berriche, An Investigation of Creep Processes in Tin and Aluminum Using Depth-Sensing Indentation Technique, *J. Mater. Res.*, Vol 7 (No. 3), 1992, p 627–638
22. M.J. Mayo and W.D. Nix, in *Proc. of the 8th Int. Conf. on the Strength of Metals and Alloys*, Pergamon Press, 1988, p 1415
23. W.H. Poisl, W.C. Oliver, and B.D. Fabes, The Relation between Indentation and Uniaxial Creep in Amorphous Selenium, *J. Mater. Res.*, Vol 10 (No. 8), 1995, p 2024–2032
24. B.N. Lucas, W.C. Oliver, J.-L. Loubet, and G.M. Pharr, Understanding Time Dependent Deformation During Indentation Testing, in *Thin Films—Stresses and Mechanical Properties VI, MRS Symposium Proc.*, Vol 436, Materials Research Society, 1997, p 233–238
25. B.N. Lucas and W.C. Oliver, Indentation Power-Law Creep of High-Purity Indium, *Metall. Mater. Trans. A*, Vol 30, 1999, p 601–610
26. G.M. Pharr, D.S. Harding, and W.C. Oliver, Measurement of Fracture Toughness in Thin Films and Small Volumes Using Nanoindentation Methods, *Mechanical Properties and Deformation Behavior of Materials Having Ultra-Fine Microstructures*, Kluwer Academic Publishers, 1993, p 449–461
27. D.S. Harding, W.C. Oliver, and G.M. Pharr, Cracking During Nanoindentation and Its Use in the Measurement of Fracture Toughness, in *Thin Films—Stresses and Mechanical Properties V, MRS Symposium Proc.*, Vol 356, Materials Research Society, 1995, p 663–668
28. A.E.H. Love, Boussinesq's Problem for a Rigid Cone, *Q. J. Math.*, Vol 10, 1939, p 161–175
29. I.N. Sneddon, The Relation Between Load and Penetration in the Axisymmetric Boussinesq Problem for a Punch of Arbitrary Profile, *Int. J. Eng. Sci.*, Vol 3, 1965, p 47–56
30. Y.-T. Cheng and C.-M. Cheng, Scaling Approach to Conical Indentation in Elastic-Plastic Solids with Work Hardening, *J. Appl. Phys.*, Vol 84, 1998, p 1284–1291
31. A. Bolshakov and G.M. Pharr, Influences of Pile-Up on the Measurement of Mechanical Properties by Load and Depth Sensing Indentation Techniques, *J. Mater. Res.*, Vol 13, 1998, p 1049–1058
32. A.K. Bhattacharya and W.D. Nix, Finite Element Simulation of Indentation Experiments, *Int. J. Solids Struct.*, Vol 24 (No. 9), 1988, p 881–891
33. A.K. Bhattacharya and W.D. Nix, Analysis of Elastic and Plastic Deformation Associated with Indentation Testing of thin Films on Substrates, *Int. J. Solids Struct.*, Vol 24 (No. 12), 1988, p 1287–1298
34. T.A. Laursen and J.C. Simo, A Study of the Mechanics of Microindentation Using Finite Elements, *J. Mater. Res.*, Vol 7, 1992, p 618–626
35. J.A. Knapp, D.M. Follstaedt, S.M. Myers, J.C. Barbour, and T.A. Friedman, Finite-Element Modeling of Nanoindentation, *J. Appl. Phys.*, Vol 85 (No. 3), 1999, p 1460–1474
36. T.Y. Tsui, W.C. Oliver, and G.M. Pharr, Indenter Geometry Effects on the Measurement of Mechanical Properties by Nanoindentation with Sharp Indenters, in *Thin Films—Stresses and Mechanical Properties VI, MRS Symposium Proc.*, Vol 436, Materials Research Society, 1997, p 147–152
37. G. Simmons and H. Wang, *Single Crystal Elastic Constants and Calculated Aggregate Properties: A Handbook*, 2nd ed., The M.I.T. Press, 1971
38. G.M. Pharr, W.C. Oliver, and F.R. Brotzen, On the Generality of the Relationship among Contact Stiffness, Contact Area, and Elastic Modulus, *J. Mater. Res.*, Vol 7 (No. 3), 1992, p 613–617
39. R.B. King, Elastic Analysis of Some Punch Problems for a Layered Medium, *Int. J. Solids Struct.*, Vol 23, 1987, p 1657–1664
40. H.J. Gao and T.-W. Wu, *J. Mater. Res.*, Vol 8 (No. 12), 1993, p 3229–3232
41. B.C. Hendrix, The Use of Shape Correction Factors for Elastic Indentation Measurements. *J. Mater. Res.*, Vol 10 (No. 2), 1995, p 255–257
42. A. Bolshakov and G.M. Pharr, Inaccuracies in Sneddon's Solution for Elastic Indentation by a Rigid Cone and Their Implications for Nanoindentation Data Analysis, in *Thin Films—Stresses and Mechanical Properties VI, MRS Symposium Proc.*, Vol 436, Materials Research Society, 1997, p 189–194
43. J.C. Hay, A. Bolshakov, and G.M. Pharr, A Critical Examination of the Fundamental Relations in the Analysis of Nanoindentation Data, *J. Mater. Res.*, Vol 14 (No. 6), 1999, p 2296–2305
44. J.C. Hay, A. Bolshakov, and G.M. Pharr, Applicability of Sneddon Relationships to the Real Case of a Rigid Cone Penetrating an Infinite Half Space, in *Fundamentals of Nanoindentation and Nanotribology, MRS Symposium Proc.*, Vol 522, Materials Research Society, 1998, p 263–268
45. J.C. Hay and G.M. Pharr, Experimental Investigations of the Sneddon Solution and an Improved Solution for the Analysis of Nanoindentation Data, in *Fundamentals of Nanoindentation and Nanotribology, MRS Symposium Proc.*, Vol 522, Materials Research Society, 1998, p 39–44
46. A. Bolshakov, W.C. Oliver, and G.M. Pharr, An Explanation for the Shape of Nanoindentation Unloading Curves Based on Finite Element Simulation, in *Thin Films—Stresses and Mechanical Properties V, MRS Symposium Proc.*, Vol 356, Materials Research Society, 1995, p 675–680
47. J.B. Pethica and W.C. Oliver, Tip Surface Interactions in STM and AFM, *Phys. Scr. Vol. T*, Vol 19, 1987, p 61
48. J.B. Pethica and W.C. Oliver, Mechanical Properties of Nanometer Volumes of Material: Use of the Elastic Response of Small Area Indentations, in *Thin Films—Stresses and Mechanical Properties, MRS Symposium Proc.*, Vol 130, Materials Research Society, 1989, p 13–23
49. B.N. Lucas, W.C. Oliver, and J.E. Swindeman, The Dynamics of Frequency-Specific, Depth-Sensing Indentation Testing, *Fundamentals of Nanoindentation and Nanotribology, MRS Symposium Proc.*, Vol 522, Materials Research Society, 1998, p 3–14
50. T.F. Page, G.M. Pharr, J.C. Hay, W.C. Oliver, B.N. Lucas, E. Herbert, and L. Riester, Nanoindentation Characterization of Coated Systems: $P:S^2$—A New Approach Using the Continuous Stiffness Technique, in *Fundamentals of Nanoindentation and Nanotribology, MRS Symposium Proc.*, Vol 522, Materials Research Society, 1998, p 53–64
51. K.W. McElhaney, J.J. Vlassak, and W.D. Nix, Determination of Indenter Tip Geometry and Indentation Contact Area

for Depth-Sensing Indentation Experiments, *J. Mater. Res.*, Vol 13 (No. 5), 1998, p 1300–1306

52. B. Taljat, T. Zacharia, and G.M. Pharr, Pile-Up Behavior of Spherical Indentations in Engineering Materials, in *Fundamentals of Nanoindentation and Nanotribology, MRS Symposium Proc.*, Vol 522, Materials Research Society, 1998, p 33–38
53. J.L. Hay, W.C. Oliver, A. Bolshakov, and G.M. Pharr, Using the Ratio of Loading Slope and Elastic Stiffness to Predict Pile-Up and Constraint Factor During Indentation, in *Fundamentals of Nanoindentation and Nanotribology, MRS Symposium Proc.*, Vol 522, Materials Research Society, 1998, p 101–106
54. Standard Test for Microhardness of Materials, "ASTM Standard Test Method E 384," *Annual Book of Standards 3.01*, American Society for Testing and Materials, 1989, p 469
55. P.J. Burnett and D.S. Rickerby, The Mechanical Properties of Wear Resistant Coatings 1: Modeling of Hardness Behaviour, *Thin Solid Films*, Vol 148, 1987, p 41–50
56. P.J. Burnett and D.S. Rickerby, The Mechanical Properties of Wear Resistant Coatings 2, *Thin Solid Films*, Vol 148, 1987, p 51–65
57. B. Jonsson and S. Hogmark, *Thin Solid Films*, Vol 114, 1984, p 257
58. T.Y. Tsui, W.C. Oliver, and G.M. Pharr, Nanoindentation of Soft Films on Hard Substrates—The Importance of Pileup, in *Thin Films—Stresses and Mechanical Properties VI, MRS Symposium Proc.*, Vol 436, 1997, p 207–212
59. T.Y. Tsui, C.A. Ross, and G.M. Pharr, Nanoindentation Hardness of Soft Films on Hard Substrates: Effects of the Substrate, in *Materials Reliability in Microelectronics VII, MRS Symposium Proc.*, Vol 473, 1997, p 57–62
60. B.D. Fabes and W.C. Oliver, Mechanical Properties of Coating and Interfaces, in *Thin Films—Stresses and Mechanical Properties II, MRS Symposium Proc.*, Vol 188, 1990, p 127–132
61. H. Gao, C.-H. Chiu, and J. Lee, Elastic Contact Versus Indentation Modeling of Multi-Layered Materials, *Int. J. Solids Struct.*, Vol 29 (No. 20), 1992, p 2471–2492
62. D.S. Stone, *J. Electron. Packaging*, Vol 112, 1990, p 41
63. H.Y. Yu, S.C. Sanday, and B.B. Rath, The Effect of Substrate on the Elastic Properties of Films Determined by the Indentation Test—Axisymmetric Boussinesq Problem, *J. Mech. Phys. Solids*, Vol 38, 1990, p 745–764
64. J. Mencik, D. Munz, E. Quandt, E.R. Weppelmann, and M.V. Swain, Determination of Elastic Modulus of Thin Layers Using Nanoindentation, *J. Mater. Res.*, Vol 12 (No. 9), 1997, p 2475–2484
65. T.Y. Tsui and G.M. Pharr, Substrate Effects on Nanoindentation Mechanical Property Measurement of Soft Films on Hard Substrates, *J. Mater. Res.*, Vol 14, 1999, p 292–301
66. G.M. Pharr, A. Bolshakov, T.Y. Tsui, and J.C. Hay, Nanoindentation of Soft Films on Hard Substrates: Experiments and Finite Element Simulations, in *Thin Films—Stresses and Mechanical Properties VII, MRS Symposium Proc.*, Vol 505, 1998, p 109–120
67. J.C. Hay and G.M. Pharr, Critical Issues in Measuring the Mechanical Properties of Hard Films on Soft Substrates by Nanoindentation Techniques, in *Thin Films—Stresses and Mechanical Properties VII, MRS Symposium Proc.*, Vol 505, 1998, p 65–70
68. A.G. Atkins, A. Silverio, and D. Tabor, Indentation Creep, *J. Inst. Metals*, Vol 94, 1966, p 369–378
69. D.S. Stone and K.B. Yoder, Division of the Hardness of Molybdenum into Rate-Dependent and Rate-Independent Components, *J. Mater. Res.*, Vol 9 (No. 10), 1994, p 2524–2533
70. D. Tabor, *Hardness of Metals*, Oxford University Press, 1951, p 46, 67–83, 105–106
71. K.L. Johnson, *Contact Mechanics*, Cambridge University Press, 1985, p 94, 176
72. W.B. Morton and L.J. Close, Notes on Hertz' Theory of Contact Problems, *Philos. Mag.*, Vol 43, 1922, p 320
73. R.M. Davies, The Determination of Static and Dynamic Yield Stresses Using a Steel Ball, *Proc. R. Soc. (London) A*, Vol 197, 1949, p 416
74. "Standard Methods of Preparation of Metallographic Specimens," E 380, *Annual Book of ASTM Standards*, ASTM, reapproved 1993

J. Mencik and M.V. Swain, Errors Associated with Depth-Sensing Microindentation Tests, *J. Mater. Res.*, Vol 10 (No. 6), 1995, p 1491–1501